

Fourier transform spectrometry without Fourier analysis of the interferogram

Miguel Lagos¹, Rodrigo Paredes² and César Retamal³

¹ Departamento de Tecnologías Industriales, Facultad de Ingeniería, Universidad de Talca, Campus Los Niches, Camino a Los Niches km 1, Curicó, Chile.

² Departamento de Ciencias de la Computación, Facultad de Ingeniería, Universidad de Talca, Campus Los Niches, Camino a Los Niches km 1, Curicó, Chile.

³ Departamento de Ciencias de la Construcción, Facultad de Ingeniería, Universidad de Talca, Campus Los Niches, Camino a Los Niches km 1, Curicó, Chile.

E-mail: mlagos@utalca.cl

Abstract. It is shown here that precision is gained by analyzing the interferometric spectra directly from the interferograms, with no previous Fourier transformation to put them in the standard frequency domain. The method is based on the theoretical calculation of the lineshape, which gives a general closed-form expression for the spectrum in the time domain and is directly assimilable to the experimental interferogram. Error sources in Fourier integrals, apodization, peak fitting with standard interpolation functions, choice of background level, Stokes energy shifts, etc., are neatly avoided.

Keywords: optical spectra, FTIR spectroscopy, quantum optics, chemical analysis

1. Introduction

We show here the scientific basis for an alternate way to process the raw data constituting the output of Fourier transform spectrometers, which is expected to improve substantially the precision of both concentration and energy measurements. In a standard traditional dispersive spectrometer, good frequency resolution is attained at the cost of blocking by the narrow slit of the monochromator most of the photons that otherwise would reach the detector. This brings down the signal to noise ratio. A Fourier transform spectrometer replaces the monochromator by a Michelson interferometer which yields the cosine Fourier transform of the spectrum as the output. The procedure collects information at all frequencies simultaneously (multiplex advantage), improving dramatically both speed and signal to noise ratio because the detector captures the full intensity of the light coming from the sample (throughput advantage). The output is an interferogram consisting on a graph giving the radiation intensity as a function of the difference in the optical path length of the two arms of the interferometer,

which is accurately measured from the interference fringes of a reference laser (Connes advantage). It is referred to as the raw data, and usually exhibits a complex oscillating structure which must be Fourier transformed to bring out the spectrum in conventional way. The spectrometer then has to be associated to a numerical processor to display the spectrum. Infrared (IR) absorption spectroscopy went through a major advance when Fourier transform spectroscopy (FTIR) came to the fore, and practically no dispersive IR equipment is in the market today. However the procedure is also practical in optical spectroscopy, nuclear magnetic resonance spectroscopy and magnetic resonance spectroscopic imaging [1, 2, 3].

However, the numerical integration of strongly oscillating functions may give large errors and hence performing the Fourier transform of the raw data to display the spectrum in conventional way may be not a minor task. By this reason, the feasibility of the new technique was associated to the development of a mathematical method for the fast calculation of the Fourier transform of highly structured functions (the FFT algorithm). The discovery of this method by Cooley and Tukey in 1965 initiated a new generation of IR instruments and techniques [4]. Anyway, processing of the raw data to display a standard spectrum involves some error. Beside the numeric errors, it is also necessary to control spurious spectral features created by the truncation of the interferogram constituting the raw data. Experimental scans are necessarily finite, and the sudden cutoffs at the boundaries have broad Fourier representations which must be recognized and discarded by a procedure known as apodization. Hence the Fourier transform of the raw data constitutes the first main source of error.

The other source of error is the little attention usual methods gives to the precise physical origin of line shapes, broadenings and shifts. Precise quantitative chemical analysis and the accurate determination of the excitation energies of molecular bonds demand more elaborate mathematical processing of the spectra, additional to the Fourier transformation of the raw data. The concentration of a chemical species is determined by the area under the peak identifying a characteristic bond of it, whose evaluation demands curve fitting of the data, particularly in the presence of heavy overlapping or structured background. Gauss, Lorentz and Voigt distributions are in practice the analytical expressions used for fitting the shape of the spectral peaks and determining their areas by integration. However, these distributions are merely interpolation functions because, in rigor, do not follow from solving a real physical model for the processes causing the peak broadenings [5]. Gauss and Lorentz curves are analytically very different, especially concerning the contribution of the tails to the peak area, which is much more significant for the latter. Tails immerse in the noisy background and their effect owns to the domain of experimental uncertainty when using a tentative model for the lineshape. It has been proven that the assigned peak intensities may show substantial variations with the choice of the lineshape model [6]. The symmetry of these standard distributions evidences their limited ability to describe spectral profiles. It has been demonstrated on a general basis that the lineshapes for photon absorption and emission by atomic or molecular species in a condensed environment are always asymmetric with respect to the net energy of

the electronic transition [7, 8]. Hence a second main source of error is the adoption of a standard distribution not well grounded on the physics of the target to describe the spectral features. The fit of the experimental data by the mathematical curves given by a realistic model for the profiles of the spectral features greatly improves precision. If the theoretical curve reproduces well the physics of the radiation field interacting with the target then the error is given by the statistical dispersion of the experimental points along the curve that bests the fit, instead of its whole breadth [7, 8, 9, 10, 11].

2. Lineshape functions of electromagnetic spectra

Line broadenings and energy shifts are produced mainly by multiphonon processes involving the extended acoustic modes of vibration of the condensed medium embedding the photosensitive orbital. They are activated by the local distortion that follows the sudden excitation or de-excitation of the electronic bonding orbitals, and can be calculated analytically, yielding a closed-form mathematical expression for the lineshape function [7, 8]. It is fortunate that this theoretical expression for the spectral distribution in the standard frequency domain has the general form of the Fourier transform of a function in the time domain. This way, the theory gives directly what experimentalists call the *raw data* and there is no need in principle of calculating the Fourier transforms of the theoretical and experimental results to compare them and make them to fit. The first and second main sources of error are thus avoided by making the theoretical analysis of the spectra in the time domain, working directly with the raw data.

The lineshape function has been proven in the recent literature to be given by the integral expression [7, 8, 9, 11]

$$F(\hbar ck; T) = \frac{a}{\pi \hbar v_s} \int_{-\infty}^{\infty} d\tau \left\{ \exp[-\alpha J(\tau; T)] - \exp[-\alpha J(\infty; T)] \right\} \\ \times \exp \left\{ i \left[\alpha I(\tau) - \frac{2a}{\hbar v_s} (\hbar ck - E) \tau \right] \right\} + \exp[-\alpha J(\infty; T)] \delta(\hbar ck - E), \quad (1)$$

where $\hbar ck$ is the photon energy, E the energy difference of the two electronic states involved in the transition, a is essentially the bond length, and v_s the mean speed of sound of the acoustic modes of vibration of the medium. The adimensional constants α and β , and the adimensional dummy time τ are given by

$$\alpha = \frac{3(\Delta F)^2}{\pi^2 \hbar \rho v_s^3} \quad \beta = \frac{\hbar v_s}{2ak_B T} \quad \tau = \frac{v_s}{2a} t, \quad (2)$$

where ΔF is the bond mean force variation upon excitation, ρ is the density, k_B is the Boltzmann constant, and T the temperature. The auxiliary functions $J(\tau; T)$ and $I(\tau)$ are dependent on the symmetry of the surroundings of the orbital undergoing the transition. For the simplest case of octahedral coordination (OC) of the optically active orbital they read

$$J(\tau; T) = \int_0^{aqD} \frac{dx}{x} \left(1 - \frac{\sin x}{x} \right) \coth(\beta x) \sin^2(\tau x) \quad (\text{OC}) \quad (3)$$

$$I(\tau) = \frac{1}{2} \int_0^{aq_D} \frac{dx}{x} \left(1 - \frac{\sin x}{x}\right) \sin(2\tau x) \quad (\text{OC}), \quad (4)$$

with q_D being the Debye wavevector of the acoustic waves, $aq_D = (12\pi^2)^{1/3}$, and

$$J(\infty; T) = \frac{1}{2} \int_0^{aq_D} \frac{dx}{x} \left(1 - \frac{\sin x}{x}\right) \coth(\beta x) \quad (\text{OC}). \quad (5)$$

The second term in the right hand side of Eq. (1) for $F(\hbar ck; T)$, containing the delta-function, is the zero-phonon line, and the first one is the phonon broadened distribution. The lineshape function $F(\hbar ck; T)$ is normalized as [9, 7, 8]

$$\int_{-\infty}^{\infty} d(\hbar ck) F(\hbar ck; T) = 1 \quad (6)$$

and hence the relative contribution of zero-phonon processes to the total is $I_{ZPL} = \exp[-\alpha J(\infty; T)]$.

Other symmetries may give more complicated functional forms for J and I . For example, for tetrahedral coordination (TC) of the optically active orbitals one has that

$$J(\tau; T) = \int_0^{aq_D} \frac{dx}{x} \left[\frac{5}{2} - \frac{3 \sin x}{2x} - \frac{\sin\left(\frac{1}{2}\sqrt{3}x\right)}{\frac{1}{2}\sqrt{3}x} \right] \coth(\beta x) \sin^2(\tau x) \quad (\text{TC}), (7)$$

$$I(\tau) = \frac{1}{2} \int_0^{aq_D} \frac{dx}{x} \left[\frac{5}{2} - \frac{3 \sin x}{2x} - \frac{\sin\left(\frac{1}{2}\sqrt{3}x\right)}{\frac{1}{2}\sqrt{3}x} \right] \sin(2\tau x) \quad (\text{TC}). \quad (8)$$

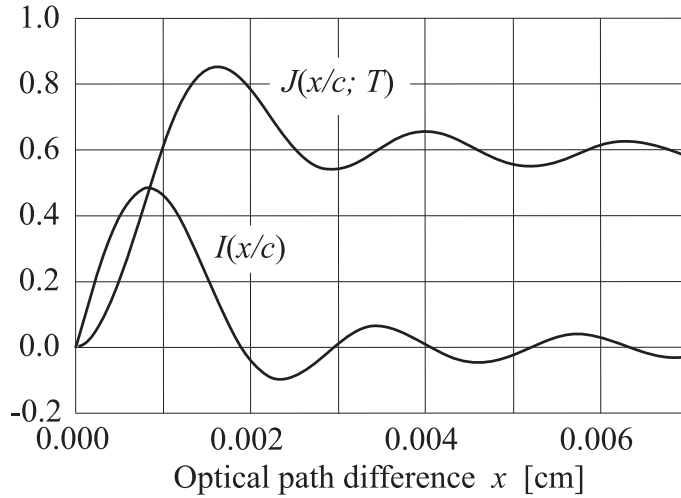


Figure 1. The auxiliary functions $J(x/c; T)$ and $I(x/c)$ defined in Eqs. (3) and (4) for octahedral symmetry with $\tau = x/c$.

The output $f(x, T)$ of the Michelson interferometer, where x is the difference in the optical path lengths of the two arms of the interferometer, is the cosine Fourier transform of the spectrum given by the lineshape function (1), i. e.

$$f(x; T) = hc \int_{-\infty}^{\infty} d\bar{k} F(\hbar c\bar{k}; T) [1 + \cos(2\pi i\bar{k}x)], \quad (9)$$

where $\bar{k} = 1/\lambda$ is the wave number and h the Planck constant. Substituting Eq. (1) and solving the integral this gives

$$f(x; T) = 1 + \exp \left[-\alpha J \left(\frac{x}{c}; T \right) \right] \cos \left[\alpha I \left(\frac{x}{c} \right) + \frac{Ex}{\hbar c} \right], \quad (10)$$

where x in fact plays the role of the virtual time $t = x/c$, conjugate to the angular frequency $\omega = E/\hbar$. Function $f(x; T)$ is actually the interferogram which FTIR spectroscopists call the *raw data*. Therefore, replacing in Eq. (10) the pairs of auxiliary functions (3) and (4) for octahedral symmetry of the optically active orbitals, or (7) and (8) for tetrahedral coordination of them, one obtains explicit closed-form mathematical expressions for the interferograms. Auxiliary functions for other symmetries can be derived from the general expressions for the electron-phonon coefficients, given in Ref. [8].

3. The proposed method

As both the experimental technique and the general theory, which is well grounded on the physics of the energy transfers between the radiation field and the charges in a condensed system, arrive both to the interferogram expressed by Eq. (10), in principle there is no need to perform any Fourier transform of the data to grasp the physical information from the experimental results. The analytical closed-form expression (10) depends on only a few parameters, α , β and the net transition energy E , per spectral line. Hence the most practical way to proceed is to find the constants α , β and E by means of a best fit analysis of Eq. (10) to the experimental interferograms. Fourier analysis then becomes just an optional alternative for people which likes to identify spectra in the conventional frequency domain.

The method seems highly convenient because retains all the advantages of Fourier spectrometry avoiding the numerical errors associated to the Fourier integration of rapidly oscillating functions. An important example of this is given by the area under the spectral line, which in agreement with Eq. (9) is given by half the intensity $f(0, T)/2$ of the central maximum of the interferogram. This magnitude is unity under the hypothesis of a single emission or absorption center of our theory, but in empirical grounds is proportional to the number of optically active orbitals and gives the concentration of them. However, the implementation of practical procedures for interpreting the measured interferograms directly with Eq. (10) may be not immediate, particularly when dealing with narrow spectral lines, precisely because their interferograms oscillate strongly with x . In particular, the central maximum may be very narrow and its intensity may be strongly affected by the experimental uncertainty of x .

The general procedure can be applied to both wide spectral features, like those displayed by fluorescent compounds, or narrow ones, as the sharp minima observed in the absorption spectra of infrared light passing through many materials. The physical process is essentially the same. Figures 1, 2 and 3 show the mathematical steps of the calculation of the spectrum of YAG:Ce³⁺ (yttrium aluminum garnet, Y₃Al₅O₁₂, doped

with Ce^{3+}), a phosphor having many technical applications. This system is particularly interesting because its emission spectrum has been measured at a temperature close to $T = 0$ with a resolution large enough to clearly observe at $\lambda = 489 \text{ nm}$ ($\bar{k} = 20450 \text{ cm}^{-1}$) the zero-phonon line belonging to the main of the two emission bands [12]. The relative intensity of the zero-phonon line of $\text{YAG}:\text{Ce}^{3+}$ at temperature $T = 4 \text{ K}$ is observed to be 0.27% of the total intensity of the main emission band. The emission has been attributed to competing transitions [12, 11] of the AlO_6 groups of quasi-octahedral coordination inside the complex unit cell of YAG [13].

Fig. 1 shows the auxiliary functions $J(x/c; T)$ and $I(x/c)$ for octahedral symmetry, as given by Eqs. (3) and (4). Fig. 2 represents the theoretically predicted interferogram

$$f(x; T) = \frac{2}{3}f_1(x; T) + \frac{1}{3}f_2(x; T) \quad (11)$$

of two competing emissions with weights 2/3 and 1/3. The weighting factors follow from assuming that the quasi-octahedrally coordinated emission center has degenerate x and y lobes and slightly different z lobes. Both f_1 and f_2 have the functional form (10) with constants α , β and E chosen to fit the measured spectrum. The transition energies are $E_1 = 2.535 \text{ eV}$ and $E_2 = 2.343 \text{ eV}$ (corresponding to the wavenumbers $\bar{k}_1 = E_1/(hc) = 20450 \text{ cm}^{-1}$ and $\bar{k}_2 = E_2/(hc) = 18900 \text{ cm}^{-1}$). The other constants are $\alpha_1 = 10.00$, $\alpha_2 = 12.25$ and $\beta = \infty$ because $T \approx 0$. The value of E_1 is given by the zero-phonon line, and hence is not an adjustable parameter, the other three constants were chosen to fit the experimental data.

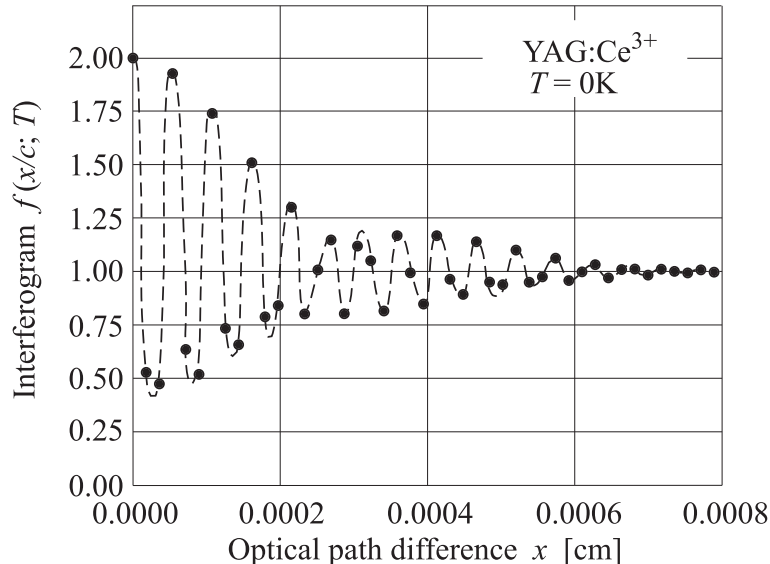


Figure 2. Filled black circles represent the function $f(x; T)$ given by Eq. (11), where f_1 and f_2 have the general form (10) with slightly different parameters α and E . It is expected that $f(x; T)$ will reproduce the experimentally registered Michelson interferogram of two partially resolved spectral features emitted by centers which have concentrations in the ratio 2:1. The broken line is only a guide to the eye.

Notice in Fig. 2 that the number of the calculated points in the interval of x where $f(x/c; T)$ is appreciable seems insufficient to represent properly the too structured function. This is not really a problem to construct the spectrum because the FFT algorithm is an analytic procedure that finds out the function whose Fourier transform (or anti-transform) passes by the given points. The main aspect is the accuracy of these points, but care must be taken also to avoid aliasing of the frequency by a poor sampling of the data.

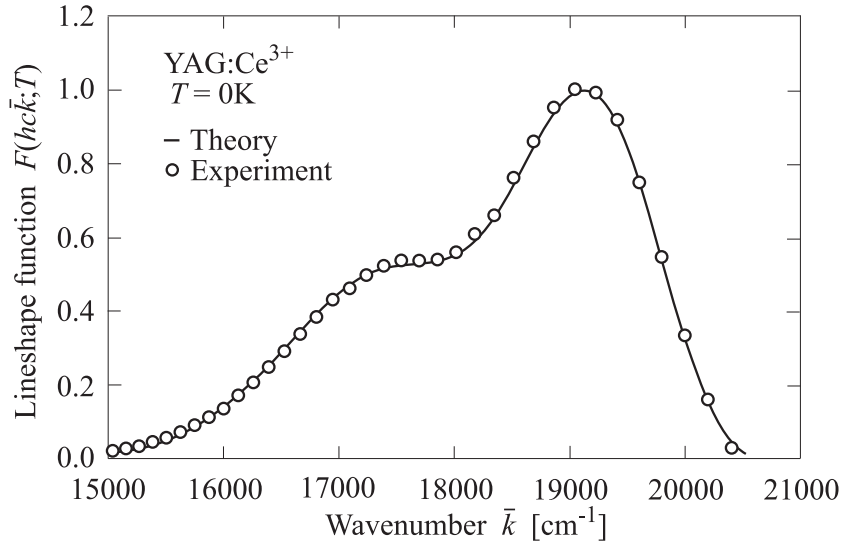


Figure 3. Open circles represent the fluorescent emission spectrum of YAG:Ce³⁺ at $T = 4$ K, as measured by Bauchmann et al. [1]. The solid line represents the Fourier transform of the function represented in Fig. 2 by the discrete set of filled black circles.

Fig. (3) shows the cosine Fourier transform of the function (11), calculated by the FFT algorithm included as a standard tool in the Excel spreadsheet. The agreement of the theoretical curve with the experimental spectrum is quite impressive. As the Fourier transform is unique, this indicates that function (11) with the assumed values for the constants should represent with good accuracy the output of the Michelson interferometer. The FFT algorithm was run with 1024 points for x , which runs over an interval of optical path differences $0 \leq x \leq 0.02$ mm.

Figure (4) shows a calculated interferogram of the general form

$$f(x; T) = \frac{3}{4}f_1(x; T) + \frac{1}{4}f_2(x; T) \quad (12)$$

where both f_1 and f_2 are given by Eq. (10) with the auxiliary functions (7) and (8) for tetrahedral symmetry. The weighting factors $3/4$ and $1/4$ assume a single distorted orbital in the subgroup of coordination four inserted in the more complex unit cell. The constants $\alpha_1 = 18$ and $\alpha_2 = 22$, and the wavenumbers $\bar{k}_1 = 20510 \text{ cm}^{-1}$ and $\bar{k}_2 = 19700 \text{ cm}^{-1}$ ($E_1 = 2.543 \text{ eV}$ and $E_1 = 2.442 \text{ eV}$), are chosen to give the fit of the experimental spectrum of Rhodamine 6G shown in Fig. 5.

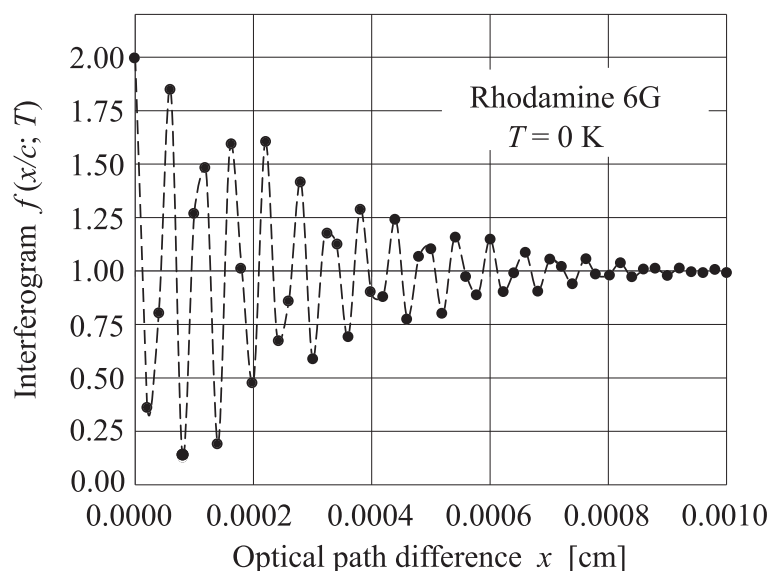


Figure 4. Black dots represent function $f(x; T)$ given by Eq. (12), where f_1 and f_2 have the general form (10) with parameters α and E chosen to fit the Michelson interferogram of Rhodamine 6G. The broken line is only a guide to the eye.

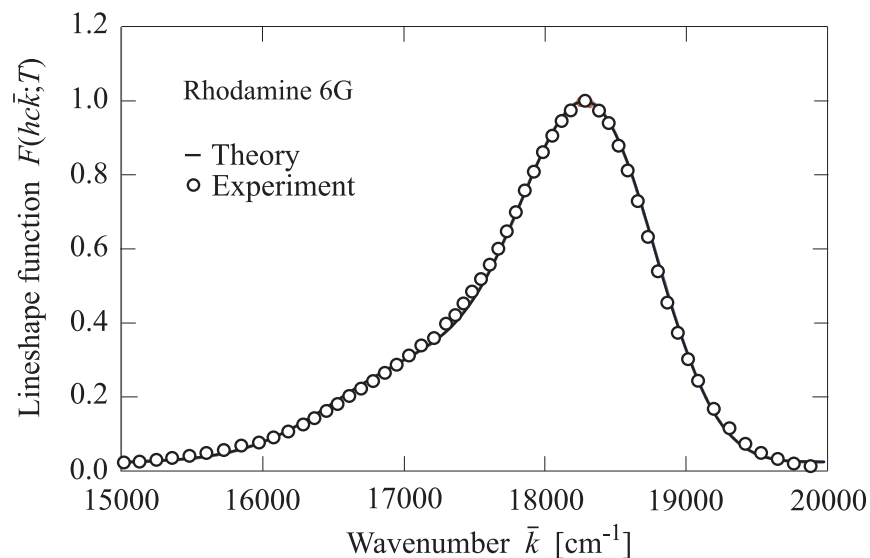


Figure 5. Open circles represent the fluorescent emission spectrum of Rhodamine 6G (Thermo Fisher Scientific, Fluorescence SpectraViewer) and the solid line corresponds to the theoretical lineshape function obtained from the Fourier transform of the function passing by the black dots of Fig. 4.

4. Conclusions

The method put forward here replaces the Fourier analysis of the interferogram given as the output of a Fourier transform spectroscope by a best fit analysis of Eq. (10) to the data. The procedure conserves all the advantages of traditional Fourier transform

spectroscopy:

(i) Throughput (or Jacquinot) advantage. The energy throughput in the interferometer is much higher than in a dispersive spectrometer because has no slit selecting a narrow wavelength interval.

(ii) Multiplex (or Fellgett) advantage. The interferometer measures all source wavelengths simultaneously and not by successive intervals, one at a time, as in a dispersive instrument. (This and the former attribute combine so that a Fourier transform spectrometer can achieve much better signal-to-noise ratio than a dispersive instrument in a shorter time).

(iii) Connes advantage. The scale for the optical path length difference of the interferometer is given by a HeNe laser, which provides a very fine, accurate and stable internal reference for each scan. This is much more accurate and has much better long term stability than the wavelength calibration of a dispersive instrument, which is essentially mechanical.

(iv) Other advantages are the absence of random scattered light in the Fourier transform spectrograph. The slit of a dispersive instrument rejects most of the incoming light, which contributes to feed a diffuse light level inside the apparatus. Also, the resolution of the interferometer is constant at all wavenumbers, whereas the lower throughput of dispersive instruments frequently obliges to adjust the slit during the scan, modifying resolution.

But adds other important advantages:

(v) Numeric errors associated to the integration of rapidly oscillating functions are avoided.

(vi) Apodization becomes unnecessary.

(vii) The procedure directly gives the net energy E released or captured by the electronic transition, with no Stokes shift.

5. References

- [1] Griffiths P R and Haseth J A 1986 *Fourier Transform Infrared Spectrometry* 2nd ed (New York: Wiley).
- [2] Stuart B 2004 *Infrared Spectroscopy: Fundamentals and Applications* (New York: Wiley).
- [3] Hlivko B, Hong H and Williams R R 1988 *Appl. Spectrosc.* **42** 1563–1566.
- [4] Cooley J W and Tukey J W 1965 *Math. Comput.* **19** 297–301.
- [5] Dodd J G and DeNoyer 2002 L K in *Handbook of Vibrational Spectroscopy* ed. by Chalmers J M and Griffiths P R (Chichester: Wiley).
- [6] Marshall I, Bruce S D, Higinbotham J, MacLulich A, Wardlaw J M, Ferguson K J and Seck J 2000 *Magnetic Resonance in Medicine* **44** 646–649.
- [7] Lagos M, Asenjo F, Hauyón R, Pastén D, González H, Henríquez R and Troncoso R 2008 *Phys. Rev. B* **77** 104305.
- [8] Lagos M, Asenjo F, Hauyón R, Pastén D and Moya P S 2010 *J. Phys. Chem. A* **114** 7353–7358.
- [9] Lagos M and Paredes R 2014 *J. Phys. Chem. A* **118** 10754–10762.
- [10] Lagos M and Paredes R 2016 *Solid State Commun.* **242** 52–56.
- [11] Lagos M, Paredes R and Retamal C 2017 *J. Photochem. Photobiol. A* **344** 344, 163–167.
- [12] Bachmann V, Ronda C and Meijerink A 2009 *Chem. Mater.* **21** 2077–2084.

- [13] Gracia J, Seijo L, Barandiarán Z, Curulla D, Niemansverdriet H and van Gennip W 2008 *J. Lumin.* **128** 1248–1254.